


 Cite this: *Phys. Chem. Chem. Phys.*,  
2016, 18, 9922

 Received 25th February 2016,  
Accepted 18th March 2016

DOI: 10.1039/c6cp01279e

www.rsc.org/pccp

## Saturn-like charge-transfer complexes $\text{Li}_4\text{B}_{36}$ , $\text{Li}_5\text{B}_{36}^+$ , and $\text{Li}_6\text{B}_{36}^{2+}$ : exohedral metalloborospherenes with a perfect cage-like $\text{B}_{36}^{4-}$ core†

 Wen-Juan Tian, Qiang Chen, Hai-Ru Li, Miao Yan, Yue-Wen Mu, Hai-Gang Lu,\*  
Hua-Jin Zhai\* and Si-Dian Li\*

Based on extensive first-principles theory calculations, we present the possibility of construction of the Saturn-like charge-transfer complexes  $\text{Li}_4\text{B}_{36}$  (2),  $\text{Li}_5\text{B}_{36}^+$  (3), and  $\text{Li}_6\text{B}_{36}^{2+}$  (4) all of which contain a perfect cage-like  $\text{B}_{36}^{4-}$  (1) core composed of twelve interwoven boron double chains with a  $\sigma + \pi$  double delocalization bonding pattern, extending the  $\text{B}_n^q$  borospherene family from  $n = 38\text{--}42$  to  $n = 36$  with the highest symmetry of  $T_h$ .

As a typical electron-deficient element, boron has a rich chemistry dominated by multicenter-two-electron bonds (mc-2e bonds) in both polyhedral molecules and bulk allotropes. Multicenter bonds also appear to be responsible for the planar or quasi-planar structures of a wide range of boron clusters  $\text{B}_n^{-/0}$  ( $n = 3\text{--}25, 27, 30, 35,$  and  $36$ ).<sup>1–10</sup> In particular,  $\text{B}_{36}$  possesses a high-symmetry  $C_{6v}$  quasi-planar structure featuring dual  $\pi$  aromaticity, analogous to coronene ( $\text{C}_{24}\text{H}_{12}$ ).<sup>8,9</sup> The possibility of preparation of all-boron fullerenes was firstly proposed for  $\text{B}_{80}$  in 2007,<sup>11</sup> constructed from  $\text{C}_{60}$  by capping the twenty surface hexagons. However, later theoretical investigations indicate that  $\text{B}_{80}$  strongly favors core-shell-type structures over the fullerene-like configuration.<sup>12,13</sup> The first all-boron fullerenes  $D_{2d} \text{B}_{40}^{-/0}$ , referred to as borospherenes in the literature, were discovered in 2014 in a combined experimental and theoretical investigation.<sup>14</sup> The axially chiral borospherenes  $C_3/C_2 \text{B}_{39}^-$  were observed in 2015.<sup>15</sup> Two cationic chiral members  $C_1 \text{B}_{41}^+$  and  $C_2 \text{B}_{42}^{2+16}$  were recently presented to the borospherene family based on extensive first-principles theory calculations. The cubic-box-like  $\text{B}_{39}^-, \text{B}_{40}, \text{B}_{41}^+,$  and  $\text{B}_{42}^{2+}$  thus form a  $\pi$ -isovalent  $\text{B}_n^q$  series in different charge states ( $q = n - 40$ ), which are all composed of twelve interwoven boron double-chains (BDCs) with six hexagonal or heptagonal faces, that is,  $n_6 + n_7 = 6$  with (3, 3), (2, 4), (1, 5), and (0, 6) for  $n = 39, 40, 41,$  and  $42$ , respectively. Multicenter bonding interactions go extreme in these borospherenes which possess the universal bonding pattern of  $\sigma$  plus  $\pi$  double

delocalization, with 12 multicenter two-electron  $\pi$ -bonds (12 mc-2e  $\pi$ ) over a  $\sigma$ -skeleton made of  $n + 8$  delocalized three-center-two-electron  $\sigma$ -bonds ( $n + 8$  3c-2e  $\sigma$ ).<sup>14–16</sup> The observation of  $D_{2d} \text{B}_{40}^{-/0}$  and  $C_3/C_2 \text{B}_{39}^-$  leads to a quick surge of borospherene chemistry. The first endohedral  $\text{M}@\text{B}_{40}$  ( $\text{M} = \text{Ca}, \text{Sr}$ ) and exohedral  $\text{M}@\text{B}_{40}$  ( $\text{M} = \text{Be}, \text{Mg}$ ) metalloborospherenes were reported in a recent communication at the density functional theory (DFT) level.<sup>17</sup> A theoretical study of the electronic structure and electronic spectra of  $D_{2d} \text{B}_{40}$ ,<sup>18</sup> a topological analysis of  $D_{2d} \text{B}_{40}$ ,<sup>19</sup> a computational investigation on endohedral  $\text{M}@\text{B}_{40}$  ( $\text{M} = \text{Sc}, \text{Y}, \text{La}$ ),<sup>20</sup> a molecular dynamics study of  $D_{2d} \text{B}_{40}$  at high temperatures,<sup>21</sup> and a theoretical prediction of the hydrogen-storage capacity of  $\text{B}_{40}$ <sup>22</sup> quickly followed. Both  $\text{B}_{38}^{2-}$  and  $\text{B}_{39}^-$  borospherenes have also been stabilized in  $\text{Ca}@\text{B}_{38}$ <sup>23</sup> and  $\text{Ca}@\text{B}_{39}$ <sup>24</sup> by encapsulating a Ca atom at the cage center as an electron donor.  $C_2/C_s \text{B}_{42}^+$  borospherenes with octagonal holes were also reported.<sup>25</sup> The latest development in boron clusters is the characterization of the seashell-like  $C_2 \text{B}_{28}^{-/0}$  which, as the smallest borospherenes observed so far in a structural pattern different from  $D_{2d} \text{B}_{40}$ , possesses one surface hexagon and two surface heptagons with  $(n_6, n_7) = (1, 2)$ .<sup>26</sup> However, there have been no borospherenes reported to date with purely surface hexagons. Whether a cubic-box-like  $\text{B}_n^q$  borospherene with six surface hexagons and no heptagon  $(n_6, n_7) = (6, 0)$  exists or not or whether such an electron-deficient cage can be effectively stabilized with metal dopants as electron donors remains an open question in both experiment and theory.

Based on extensive first-principles theory calculations, we present herein the possibility of the construction of Saturn-like  $\text{Li}_4\text{B}_{36}$  (2),  $\text{Li}_5\text{B}_{36}^+$  (3), and  $\text{Li}_6\text{B}_{36}^{2+}$  (4) which, as typical exohedral charge-transfer complexes, all contain a perfect cage-like  $\text{B}_{36}^{4-}$  (1) core composed of twelve interwoven BDCs with six surface hexagons, expanding the  $\text{B}_n^q$  family to  $\text{B}_{36}^{4-}$  with  $(n_6, n_7) = (6, 0)$ . As the lowest-lying isomers of the systems obtained, the high-symmetry  $D_{2h} \text{Li}_4\text{B}_{36}$  (2),  $C_{2v} \text{Li}_5\text{B}_{36}^+$  (3), and  $T_h \text{Li}_6\text{B}_{36}^{2+}$  (4) possess 44 delocalized 3c-2e  $\sigma$  bonds and 12 delocalized 5c-2e  $\pi$  bonds evenly distributed on the cage surface, matching the  $\sigma + \pi$  double delocalization bonding pattern of the borospherene family perfectly. The vibrational frequencies and electron detachment energies of the

Nanocluster Laboratory, Institute of Molecular Science, Shanxi University,  
Taiyuan 030006, China. E-mail: luhg@sxu.edu.cn, hj.zhai@sxu.edu.cn,  
lisidian@sxu.edu.cn

† Electronic supplementary information (ESI) available. See DOI: 10.1039/c6cp01279e

concerned species have been computationally predicted to facilitate their experimental characterization.

Manual structural constructions and initial hybrid DFT-PBE0<sup>27</sup> calculations based on typical planar, cage-like, and tubular isomers of  $B_{36}^{-/0,8,9}$  were performed for  $Li_4B_{36}$ ,  $Li_5B_{36}^+$ , and  $Li_6B_{36}^{2+}$ . Extensive minima hopping (MH)<sup>13,28</sup> structural searches produced no isomers with lower energies than 2–4. Low-lying isomers were then fully optimized (with frequencies checked) with their relative energies evaluated at the DFT-PBE0 level with the 6-311+G(d) basis set<sup>29</sup> using the Gaussian 09 suite.<sup>30</sup> The relative stabilities of the important lowest-lying isomers of 2–4 were further refined using the more accurate coupled cluster method with triple excitations (CCSD(T))<sup>31–33</sup> implemented in MOLPRO<sup>34</sup> with the 6-311G(d) basis set at the PBE0 geometries. Molecular dynamics (MD) simulations were performed for 2–4 at 200, 400, 600 K, and 800 K for 30 ps using the software suite CP2K.<sup>35</sup> The optimized  $T_h B_{36}^{4-}$  (1),  $D_{2h} Li_4&B_{36}$  (2),  $C_{2v} Li_5&B_{36}^+$  (3), and  $T_h Li_6&B_{36}^{2+}$  (4) are depicted in Fig. 1. More alternative isomers are summarized Fig. S1–S4 in the ESI†

It is known that the experimentally observed  $B_{36}$  possesses a beautiful  $C_{6v}$  quasi-planar geometry with a hexagonal hole at the center, with the cubic-box-like  $C_{2h} B_{36}$  cage lying much higher in energy (by 2.84 eV at PBE0).<sup>9</sup> Detailed orbital analyses indicate that, compared with  $D_{2d} B_{40}$ , the cage-like  $C_{2h} B_{36}$  lacks four  $\pi$  valence electrons to match the  $\sigma + \pi$  double delocalization bonding pattern of borospherenes.<sup>14–16</sup> It turns out to be true that the tetraanion  $B_{36}^{4-}$  (1) with four extra electrons does possess a perfect  $T_h$  cage-like local minimum which matches both the geometrical and electronic structural patterns of borospherenes (as detailed below).  $B_{36}^{4-}$  (1) can also be viewed as a cubic-box-like cage with eight apex-sharing  $B_6$  triangles at the eight corners. However,  $T_h B_{36}^{4-}$  (1) lies much higher in energy (by 4.19 eV at PBE0) than its double-ring tubular counterpart  $D_{6d} B_{36}^{4-}$  (Fig. S1, ESI†) due to the strong Coulomb repulsion in the cage. To stabilize  $T_h B_{36}^{4-}$  (1), we introduce four  $Li^+$  counterions into the system to neutralize the extra negative charges the cage carries. Encouragingly, as shown in Fig. S2 (ESI†), the neutral exohedral  $D_{2h} Li_4&B_{36}$  (2) with four face-capping  $Li^+$  atoms appears to be almost isoenergetic with the triple-ring tubular  $C_{2h} Li_4@B_{36}$  at the PBE0 level, with a minor relative energy of 0.17 eV. More convincingly, at the more accurate CCSD(T) level which has been tested to be reliable for boron clusters in this size range,<sup>14–16</sup> the cage-like  $D_{2h} Li_4&B_{36}$  (2) turns out to be 0.10 eV more stable than its triple-ring tubular rival  $C_{2h} Li_4&B_{36}$  (Fig. S2, ESI†).  $D_{2h} Li_4&B_{36}$  (2) is therefore the most stable isomer of  $Li_4B_{36}$  obtained. Four face-capping Li atoms in  $Li_4&B_{36}$  (2) are

strongly bonded to the  $B_{36}$  core over four equivalent surface hexagons, with the binding energy of 3.27 eV per Li at PBE0.  $Li_4&B_{36}$  (2) thus forms a beautiful Saturn-like exohedral complex, with the perfect  $B_{36}^{4-}$  borospherene core surrounded by four equivalent face-capping  $Li^+$  monocations on the equator. With 44 triangles on twelve interwoven BDCs and six hexagons on the cage surface, the  $B_{36}^{4-}$  borospherene core in  $Li_4&B_{36}$  (2) follows the Euler's rule as follows:  $E$  (84 edges) =  $F$  (44 triangular + 6 hexagonal faces) +  $V$  (36 vertices) – 2. As typical positional isomers of  $Li_4&B_{36}$  (2), the third lowest-lying  $C_s Li_4&B_{36}$  with four face-capping  $Li^+$  and the fifth lowest-lying  $C_{2v} Li_3&[Li@B_{36}]$  with one encapsulated  $Li^+$  and three face-capping  $Li^+$  lie 0.04 eV and 0.21 eV higher than 2 at CCSD(T), respectively. As shown in Fig. S2 (ESI†), the low-lying isomers obtained for  $Li_4B_{36}$  within 1.6 eV all turn out to be cage-like or tubular, with the quasiplanar isomers derived from the quasiplanar  $C_{6v} B_{36}$  lying much higher in energy than 2 by at least 1.63 eV.

Introducing one or two more  $Li^+$  cations into the system is expected to further stabilize the Saturn-like metalloborospherene. It turns out to be true. As shown in Fig. S3 and S4 (ESI†), both the high-symmetry  $C_{2v} Li_5&B_{36}^+$  (3) and  $T_h Li_6&B_{36}^{2+}$  (4) with a perfect  $B_{36}^{4-}$  borospherene core are the well-defined lowest-lying isomers of the systems obtained which lie much lower in energy than other low-lying isomers. The exohedral  $Li_5&B_{36}^+$  (3) with four equivalent  $Li^+$  on the equator and one  $Li^+$  on the top possesses the overall symmetry of  $C_{2v}$ , while the exohedral  $Li_6&B_{36}^{2+}$  (4) with six equivalent  $Li^+$  cations over the cage surface (with four on the equator and two on the top and bottom) has a perfect cage-like geometry with the highest symmetry of  $T_h$ .  $C_{2v} Li_4&[Li@B_{36}]^+$ , the second lowest-lying isomer of  $Li_5B_{36}^+$  with one encapsulated  $Li^+$  at the center and four face-capping  $Li^+$  on the equator lies 0.39 eV higher than  $Li_5&B_{36}^+$  (3) at CCSD(T) (Fig. S3, ESI†), while  $C_{2v} Li_5&[Li@B_{36}]^{2+}$ , the second lowest-lying isomer of  $Li_6B_{36}^{2+}$  with one encapsulated  $Li^+$  at the center, four face-capping  $Li^+$  on the equator, and one  $Li^+$  on the top, lies 0.72 eV higher in energy than  $Li_6&B_{36}^{2+}$  (4) at the same theoretical level (Fig. S4, ESI†). Other tubular and planar isomers turn out to be much less stable than 3 and 4 in thermodynamics.

The high stabilities of  $Li_4&B_{36}$  (2),  $Li_5&B_{36}^+$  (3), and  $Li_6&B_{36}^{2+}$  (4) originate from their unique electronic structures and bonding patterns. Molecular orbital analyses indicate that the closed-shell 2, 3, and 4 possess the huge HOMO–LUMO energy gaps of 2.98, 3.12, and 3.21 eV at PBE0 (Fig. S5, ESI†), respectively. These values are comparable with the corresponding values of 2.89, 3.13, 3.16, 3.24, and 3.02 eV calculated for  $C_3 B_{39}^-$ ,  $D_{2d} B_{40}$ ,  $C_1 B_{41}^+$ ,  $C_2 B_{42}^{2+}$ , and  $I_h C_{60}$  at the same theoretical level, respectively,<sup>14–17</sup> well supporting the chemical stabilities of these exohedral metalloborospherenes. Natural charge analyses<sup>36</sup> reveal that 2, 3, 4 are typical charge-transfer complexes in nature, with each face-capping Li atom donating one electron to the electron-deficient  $B_{36}$  core, as indicated by the calculated natural charges of  $q_{Li} = +0.83, +0.86,$  and  $+0.89 |e|$  and  $q_{B_{36}} = -3.32, -3.30,$  and  $-3.34 |e|$  for 2, 3, and 4, respectively.

Detailed adaptive natural density partitioning (AdNDP) analyses<sup>37</sup> unveil the universal  $\sigma + \pi$  double delocalization bonding pattern of 1–4. As shown in Fig. 2, the bare  $T_h B_{36}^{4-}$  (1) has 36 3c-2e  $\sigma$  bonds

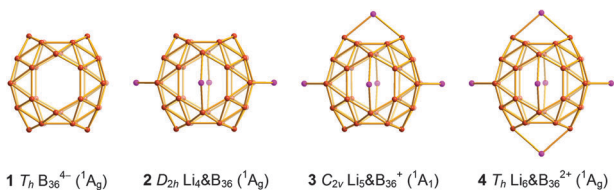


Fig. 1 Optimized structures of  $T_h B_{36}^{4-}$  (1),  $D_{2h} Li_4&B_{36}$  (2),  $C_{2v} Li_5&B_{36}^+$  (3), and  $T_h Li_6&B_{36}^{2+}$  (4) at the PBE0/6-311+G(d) level.

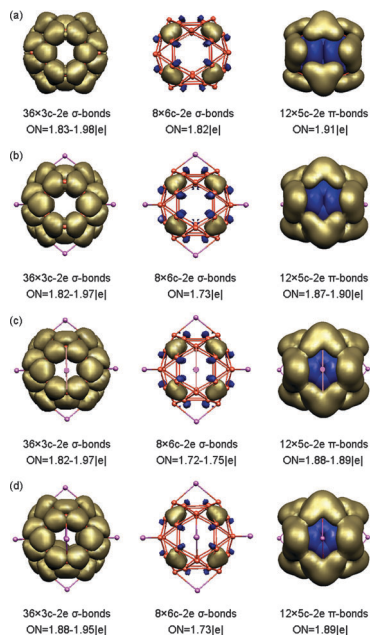


Fig. 2 AdNDP bonding patterns of (a)  $T_h B_{36}^{4-}$  (**1**), (b)  $D_{2h} Li_4@B_{36}$  (**2**), (c)  $C_{2v} Li_5@B_{36}^+$  (**3**), and (d)  $T_h Li_6@B_{36}^{2+}$  (**4**), with the occupation numbers (ONs) indicated.

evenly distributed on the 36  $B_3$  triangles on the cage surface and 8  $6c-2e$   $\sigma$  bonds on the 8  $B_6$  planar triangles at the eight corners. As the central  $B_3$  triangles make the main contributions to the  $6c-2e$   $\sigma$  bonds, these  $\sigma$  interactions can be approximately treated as 44  $3c-2e$   $\sigma$  bonds, with one  $3c-2e$   $\sigma$  bond on each  $B_3$  triangle on the cage surface. The remaining 24 valence electrons are evenly distributed in 12  $5c-2e$   $\pi$  bonds over the 12 interwoven BCDs. Such a  $\sigma + \pi$  double delocalization matches the universal bonding pattern of the borospherene family perfectly.<sup>14–17</sup> As also shown in Fig. 2, the Li-stabilized  $D_{2h} Li_4@B_{36}$  (**2**),  $C_{2v} Li_5@B_{36}^+$  (**3**), and  $T_h Li_6@B_{36}^{2+}$  (**4**) all have 36  $3c-2e$   $\sigma$  bonds, 8  $6c-2e$   $\sigma$  bonds, and 12  $5c-2e$   $\pi$  bonds. They possess therefore the same bonding pattern as  $B_{36}^{4-}$  (**1**) which, stabilized in **2–4** by 4–6 face-capping  $Li^+$  monocations, forms the smallest borospherene with the highest symmetry of  $T_h$  in the  $B_n^q$  ( $q = n - 40$ ) series.<sup>14–16</sup> Such a double delocalization bonding pattern renders three-dimensional (3D) aromaticity to these isovalent systems, as evidenced by the calculated huge negative nucleus-independent chemical shifts (NICS)<sup>38</sup> of  $-35.9$ ,  $-42.8$ ,  $-44.0$ , and  $-45.2$  ppm at the cage centers of **1**, **2**, **3**, and **4**, respectively. These numbers are well comparable with the corresponding values of  $-37$  ppm,  $-38$  ppm,  $-39$  ppm,  $-43$  ppm,  $-41$  ppm, and  $-40$  ppm calculated for  $C_s B_{38}^{2-}$ ,  $C_3 B_{39}^-$ ,  $C_2 B_{39}^-$ ,  $D_{2d} B_{40}$ ,  $C_1 B_{41}^+$ , and  $C_2 B_{42}^{2+}$ ,<sup>14–16,23</sup> respectively.

Extensive molecular dynamics simulations indicate that  $D_{2h} Li_4@B_{36}$  (**2**),  $C_{2v} Li_5@B_{36}^+$  (**3**), and  $T_h Li_6@B_{36}^{2+}$  (**4**) are dynamically highly stable at 200 K with the root-mean-square-deviations (RMSD) of RMSD = 0.06 Å, 0.07 Å, and 0.07 Å and the maximum bond length deviations of MAXD = 0.20 Å, 0.23 Å, and 0.27 Å, respectively (see Fig. S6–S8, ESI<sup>†</sup>). No obvious structural fluctuations in **2**, **3**, and **4** are seen even at 600 K. However, at 800 K,  $D_{2h} Li_4@B_{36}^{2+}$  (**2**) starts to fluctuate in concerted mechanisms involving

hexagon–heptagon structural transformations (Fig. S6, ESI<sup>†</sup>), while  $C_{2v} Li_5@B_{36}^+$  (**3**) and  $T_h Li_6@B_{36}^{2+}$  (**4**) remain dynamically stable, further indicating that the face-capping  $Li^+$  monocations help promote the structural robustness of these exohedral complexes.

Infrared photodissociation spectroscopy in combination with first-principles theory calculations has proven to be an effective approach in the characterization of novel clusters.<sup>39,40</sup> As indicated in the simulated IR spectra of **1–4** in Fig. S9 (ESI<sup>†</sup>), the two major IR peaks of  $T_h B_{36}^{4-}$  (**1**) at  $1179\text{ cm}^{-1}$  ( $t_u$ ) and  $815\text{ cm}^{-1}$  ( $t_u$ ) are well inherited in **2**, **3**, and **4**. The strong IR absorptions at  $386\text{ cm}^{-1}$  ( $b_{3u}$ ) in  $Li_4@B_{36}$  (**2**),  $357\text{ cm}^{-1}$  ( $b_2$ ) in  $Li_5@B_{36}^+$  (**3**), and  $324\text{ cm}^{-1}$  ( $t_u$ ) in  $T_h Li_6@B_{36}^{2+}$  (**4**) involve the concerted vibrations of the  $B_{36}$  core and the capping Li atoms around it. The Raman spectra of **2–4** also exhibit certain similarities to **1**, with the main peaks at  $1127\text{ cm}^{-1}$  ( $e_g$ ) and  $811\text{ cm}^{-1}$  ( $t_g$ ) in  $T_h B_{36}^{4-}$  (**1**) basically remained in **2–4** at lower relative intensities (Fig. S9, ESI<sup>†</sup>). The major Raman peaks below  $650\text{ cm}^{-1}$  in **2–4** involve the vibrations of the face-capping Li atoms in these species. The Raman active modes of  $T_h B_{36}^{4-}$  (**1**) at  $205\text{ cm}^{-1}$  ( $e_g$ ) and  $459\text{ cm}^{-1}$  ( $a_g$ ) belong to typical “radial breathing modes” (RBMs) of the  $B_{36}^{4-}$  cage. Similar RBMs exist in **2–4** with small blue shifts. A strong RBM peak was observed at  $210\text{ cm}^{-1}$  for single-walled boron nanotubes with a diameter of  $36 \pm 1\text{ \AA}$ .<sup>41</sup>

Joint photoelectron spectroscopy (PES) experimental and *ab initio* theoretical investigations have served as the most powerful approach to characterize gas-phase boron clusters in the past decade.<sup>1–10,14,15</sup> Using the time-dependent DFT approach,<sup>42</sup> we simulate the PES spectrum of  $D_{2h} Li_4@B_{36}^-$ , as shown in Fig. 3, which exhibits obvious similarities to the simulated PES of the observed  $D_{2d} B_{40}^-$ ,<sup>14</sup> with a large energy gap of 1.64 eV between the first weak peak ( $^1A_g$ ) and the second strong band ( $^3B_{3g}$ ).  $Li_4@B_{36}^-$  possesses extremely low ground-state adiabatic and vertical detachment energies ADE = 1.48 eV and VDE = 1.54 eV at PBE0, with a red-shift of about 0.9 eV with respect to  $D_{2d} B_{40}^-$ .<sup>14</sup> Other weak PES peaks with higher excitation energies may serve as fingerprints to characterize  $Li_4@B_{36}^{-/0}$  in future experiments.

Finally, we present the possibility of the Saturn-like  $D_{2h} Li_2@[Ca@B_{36}]$  (**5**),  $C_{2v} Li_3@[Ca@B_{36}]^+$  (**6**), and  $D_{2h} Li_4@[Ca@B_{36}]^{2+}$  (**7**) which possess one encapsulated  $Ca^{2+}$  at the cage center and

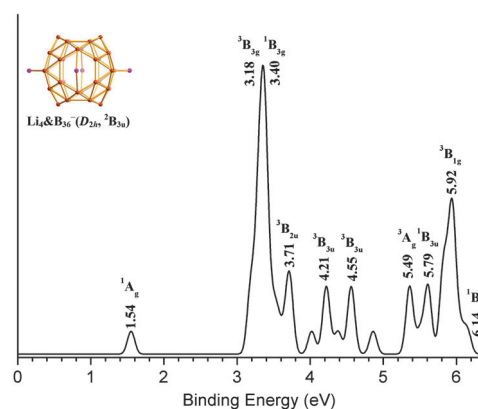


Fig. 3 Simulated PES spectrum of  $D_{2h} Li_4@B_{36}^-$ .

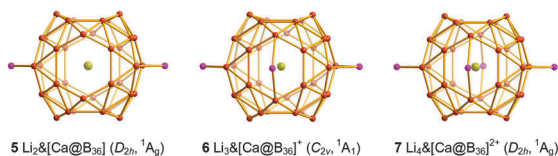


Fig. 4 Optimized structures of  $D_{2h}$   $\text{Li}_2\text{[Ca@B}_{36}\text{]}$  (5),  $C_{2v}$   $\text{Li}_3\text{[Ca@B}_{36}\text{]}^+$  (6), and  $D_{2h}$   $\text{Li}_4\text{[Ca@B}_{36}\text{]}^{2+}$  (7).

2–4  $\text{Li}^+$  monocations on the equator (Fig. 4). Calcium has proven to be an effective divalent electron donor to stabilize both  $\text{B}_{38}^{2-}$  and  $\text{B}_{39}^-$  borospherenes in  $\text{Ca@B}_{38}$  and  $\text{Ca@B}_{39}^{+2,3,24}$ . The bimetal 5–7 follow the same  $\sigma + \pi$  double delocalization bonding pattern as 2–4. They may serve as model complexes with both encapsulated and face-capping metal centers. Initial investigations indicate that  $\text{B}_{36}^{4-}$  (1) may also serve as building blocks to form  $\text{Li}_4\text{B}_{36}$  and  $\text{Ca[Ca@B}_{36}\text{]}$  3D crystals with both endohedral and exohedral metal dopants. Similarly, a  $\text{B}_{37}^{3-}$  borospherene cage may be stabilized in both  $\text{Ca@B}_{37}^-$  and  $\text{Li[Ca@B}_{37}\text{]}$ .

## Acknowledgements

This work was financially supported by the National Natural Science Foundation of China (21373130, 21573138, and 21473106).

## Notes and references

- H. J. Zhai, A. N. Alexandrova, K. A. Birch, A. I. Boldyrev and L. S. Wang, *Angew. Chem., Int. Ed.*, 2003, **42**, 6004.
- H. J. Zhai, B. Kiran, J. Li and L. S. Wang, *Nat. Mater.*, 2003, **2**, 827.
- B. Kiran, S. Bulusu, H. J. Zhai, S. Yoo, X. C. Zeng and L. S. Wang, *Proc. Natl. Acad. Sci. U. S. A.*, 2005, **102**, 961.
- W. Huang, A. P. Sergeeva, H. J. Zhai, B. B. Averkiev, L. S. Wang and A. I. Boldyrev, *Nat. Chem.*, 2010, **2**, 202.
- E. Oger, N. R. M. Crawford, R. Kelting, P. Weis, M. M. Kappes and R. Hlrichs, *Angew. Chem., Int. Ed.*, 2007, **46**, 8503.
- W. L. Li, Y. F. Zhao, H. S. Hu, J. Li and L. S. Wang, *Angew. Chem., Int. Ed.*, 2014, **53**, 5540.
- W. L. Li, Q. Chen, W. J. Tian, H. Bai, Y. F. Zhao, H. S. Hu, J. Li, H. J. Zhai, S. D. Li and L. S. Wang, *J. Am. Chem. Soc.*, 2014, **136**, 12257.
- Z. A. Piazza, H. S. Hu, W. L. Li, Y. F. Zhao, J. Li and L. S. Wang, *Nat. Commun.*, 2014, **5**, 3113.
- Q. Chen, G. F. Wei, W. J. Tian, H. Bai, Z. P. Liu, H. J. Zhai and S. D. Li, *Phys. Chem. Chem. Phys.*, 2014, **16**, 18282.
- (a) A. N. Alexandrova, A. I. Boldyrev, H. J. Zhai and L. S. Wang, *Coord. Chem. Rev.*, 2006, **250**, 2811; (b) C. Romanescu, T. R. Galeev, W. L. Li, A. I. Boldyrev and L. S. Wang, *Acc. Chem. Res.*, 2013, **46**, 350; (c) A. P. Sergeeva, I. A. Popov, Z. A. Piazza, W. L. Li, C. Romanescu, L. S. Wang and A. I. Boldyrev, *Acc. Chem. Res.*, 2014, **47**, 1349.
- N. G. Szwacki, A. Sadrzadeh and B. I. Yakobson, *Phys. Rev. Lett.*, 2007, **98**, 166804.
- F. Y. Li, P. Jin, D. E. Jiang, L. Wang, S. B. Zhang, J. J. Zhao and Z. F. Chen, *J. Chem. Phys.*, 2012, **136**, 074302.
- S. De, A. Willand, M. Amsler, P. Pochet, L. Genovese and S. Goedecker, *Phys. Rev. Lett.*, 2011, **106**, 225502.
- H. J. Zhai, Y. F. Zhao, W. L. Li, Q. Chen, H. Bai, H. S. Hu, Z. A. Piazza, W. J. Tian, H. G. Lu, Y. B. Wu, Y. W. Mu, G. F. Wei, Z. P. Liu, J. Li, S. D. Li and L. S. Wang, *Nat. Chem.*, 2014, **6**, 727.
- Q. Chen, W. L. Li, Y. F. Zhao, S. Y. Zhang, H. S. Hu, H. Bai, H. R. Li, W. J. Tian, H. G. Lu, H. J. Zhai, S. D. Li, J. Li and L. S. Wang, *ACS Nano*, 2015, **9**, 754.
- Q. Chen, S. Y. Zhang, H. Bai, W. J. Tian, T. Gao, H. R. Li, C. Q. Miao, Y. W. Mu, H. G. Lu, H. J. Zhai and S. D. Li, *Angew. Chem., Int. Ed.*, 2015, **54**, 8160.
- H. Bai, Q. Chen, H. J. Zhai and S. D. Li, *Angew. Chem., Int. Ed.*, 2015, **54**, 941.
- R. X. He and X. C. Zeng, *Chem. Commun.*, 2015, **51**, 3185.
- P. Schwerdtfeger, L. N. Wirz and J. Avery, *Wiley Interdiscip. Rev.: Comput. Mol. Sci.*, 2015, **5**, 96.
- P. Jin, Q. H. Hou, C. C. Tang and Z. F. Chen, *Theor. Chem. Acc.*, 2015, **134**, 13.
- G. Martínez-Guajardo, J. L. Cabellos, A. Díaz-Celaya, S. Pan, R. Islas, P. K. Chattaraj, T. Heine and G. Merino, *Sci. Rep.*, 2015, **5**, 11287.
- H. Dong, T. Hou, S.-T. Lee and Y. Li, *Sci. Rep.*, 2015, **5**, 9952.
- Q. Chen, H. R. Li, C. Q. Miao, Y. J. Wang, H. G. Lu, Y. W. Mu, G. M. Ren, H. J. Zhai and S. D. Li, *Phys. Chem. Chem. Phys.*, 2016, DOI: 10.1039/C5CP06169E.
- Q. Chen, T. Gao, W. J. Tian, H. Bai, S. Y. Zhang, H. R. Li, C. Q. Miao, Y. W. Mu, H. G. Lu, H. J. Zhai and S. D. Li, *Phys. Chem. Chem. Phys.*, 2015, **17**, 19690.
- T. B. Tai, S. U. Lee and M. T. Nguyen, *Phys. Chem. Chem. Phys.*, 2016, DOI: 10.1039/c5cp07342a.
- Y. J. Wang, Y. F. Zhao, W. L. Li, T. Jian, Q. Chen, X. R. You, T. Ou, X. Y. Zhao, H. J. Zhai, S. D. Li, J. Li and L. S. Wang, *J. Chem. Phys.*, 2016, **144**, 064307.
- C. Adamo and V. Barone, *J. Chem. Phys.*, 1999, **110**, 6158.
- S. Goedecker, W. Hellmann and T. Lenosky, *Phys. Rev. Lett.*, 2005, **95**, 055501.
- R. Krishnan, J. S. Binkley, R. Seeger and J. A. Pople, *J. Chem. Phys.*, 1980, **72**, 650.
- M. J. Frisch, *et al.*, *Gaussian 09, Revision D.01*, Gaussian Inc., Wallingford, CT, 2009.
- J. Čížek, *Adv. Chem. Phys.*, 1969, **14**, 35.
- G. D. Purvis and R. J. Bartlett, *J. Chem. Phys.*, 1982, **76**, 1910.
- K. Raghavachari, G. W. Trucks, J. A. Pople and M. Head-Gordon, *Chem. Phys. Lett.*, 1989, **157**, 479.
- H. J. Werner, *et al.*, *MOLPRO, version 2012.1*.
- J. VandeVondele, M. Krack, F. Mohamed, M. Parrinello, T. Chassaing and J. Hutter, *Comput. Phys. Commun.*, 2005, **167**, 103.
- E. D. Glendening, J. K. Badenhoop, A. E. Reed, J. E. Carpenter, J. A. Bohmann, C. M. Morales and F. Weinhold, *NBO 5.0*, Theoretical Chemistry Institute, University of Wisconsin, Madison, 2001.

- 37 D. Yu. Zubarev and A. I. Boldyrev, *Phys. Chem. Chem. Phys.*, 2008, **10**, 5207.
- 38 P. v. R. Schleyer and C. Maerker, *J. Am. Chem. Soc.*, 1996, **118**, 6317.
- 39 G. J. Wang, J. M. Cui, C. X. Chi, X. J. Zhou, Z. H. Li, X. P. Xing and M. F. Zhou, *Chem. Sci.*, 2012, **3**, 3272.
- 40 G. J. Wang, M. F. Zhou, J. T. Goettel, G. J. Schrobilgen, J. Su, J. Li, T. Schlöder and S. Riedel, *Nature*, 2014, **514**, 475.
- 41 D. Ciuparu, R. F. Klie, Y. M. Zhu and L. Pfefferle, *J. Phys. Chem. B*, 2004, **108**, 3967.
- 42 R. Bauernschmitt and R. Ahlrichs, *Chem. Phys. Lett.*, 1996, **256**, 454.